2009

Characterization and tuning of ultrahigh gradient permanent magnet quadrupoles

Stefan Becker
Universität Munchen, stefan.becker@physik.uni.muenchen.de

M. Bussmann
Forschungszentrum Dresden-Rossendorf FZD, m.bussmann@fzd.de

Sebastian Raith
Universität Munchen, sebastian.raith@physik.uni-muenchen.de

Matthias Fuchs
University of Nebraska - Lincoln, mfuchs@unl.edu

R. Weingartner
Max-Planck-Institut für Quantenoptik

See next page for additional authors

Characterization and tuning of ultrahigh gradient permanent magnet quadrupoles

S. Becker,[1,*] M. Bussmann,[2] S. Raith,[1] M. Fuchs,[1] R. Weingartner,[1] P. Kunz,[3] W. Lauth,[3] U. Schramm,[2] M. El Ghazaly,[3] F. Grüner,[1,4] H. Backe,[3] and D. Habs[1]

[1]*Ludwig-Maximilians-Universität München, 85748 Garching, Germany*
[2]*Forschungszentrum Dresden-Rossendorf FZD, 01314 Dresden, Germany*
[3]*Institut für Kernphysik, Universität Mainz, 55099 Mainz, Germany*
[4]*Max-Planck-Institut für Quantenoptik, 85748 Garching, Germany*

(Received 13 February 2009; published 19 October 2009)

The application of quadrupole devices with high field gradients and small apertures requires precise control over higher order multipole field components. We present a new scheme for performance control and tuning, which allows the illumination of most of the quadrupole device aperture because of the reduction of higher order field components. Consequently, the size of the aperture can be minimized to match the beam size achieving field gradients of up to 500 $\mathrm{T\,m^{-1}}$ at good imaging quality. The characterization method based on a Hall probe measurement and a Fourier analysis was confirmed using the high quality electron beam at the Mainz Microtron MAMI.

DOI: 10.1103/PhysRevSTAB.12.102801 PACS numbers: 41.85.Lc, 52.38.Kd

I. INTRODUCTION

High field gradient compact quadrupole devices have recently been the subject of an increasing amount of attention, in particular, as a compact element for beam manipulation in laser based particle acceleration. Permanent magnet quadrupole devices (PMQs) with a small aperture can reach high magnetic field gradients because of maintaining high surface magnetization. A number of design approaches have been developed and realized such as pure PMQs [1,2] in accordance with a Halbach design [3] or as modified (hybrid) Halbach quadrupole devices utilizing saturated iron to guide the magnetic field [4,5].

While being of importance in compact accelerator setups, the main interest in PMQs lies in focusing particle beams of high divergence such as laser accelerated ion beams [6] and electron beams [7–9]. The control of the field quality as introduced in this work opens the path for using PMQs as focusing elements in free-electron lasers [10] having a demand on high quality beam transport systems. Multipole field components higher than the quadrupole field component have distorting effects on the electron beam and therefore increase the beam emittance. These higher order multipole field components (HOMFC) have to be minimized.

Assuming a constant ratio of the HOMFC and the pure quadrupole field component at a given radius, small aperture approaches typically suffer from a strong influence of the HOMFC on the beam quality as the beam size to aperture is large compared to commonly used electromagnetic quadrupole devices.

We present a method of tuning PMQs in order to achieve control over higher order field components; this allows the significant reduction of HOMFC and thus allows a large ratio of beam size to aperture.

Halbach-type PMQs where built using 12 wedges (Fig. 1). The permanent magnet material is NdFeB [11] with a remanent field of 1.3 T. The assembled PMQ reaches surface magnetization fields of 1.5 T. The ability to reduce the aperture size compared to electromagnetic quadrupole devices allows the realization of field gradients of up to 500 $\mathrm{T\,m^{-1}}$ at an aperture diameter of 6 mm. Conventional electromagnetic quadrupole devices require a larger aperture and yield thus gradients of typically only 50 $\mathrm{T\,m^{-1}}$. These devices, however, usually allow the gradient to be adjusted which is not possible with a simple approach using PMQs. The PMQs as applied here were preliminarily tested and presented in [1].

Small apertures pose challenges in the measurement of the magnetic field distribution within. Common approaches involve the application of Hall probes to determine the field gradients or rotating coils to determine

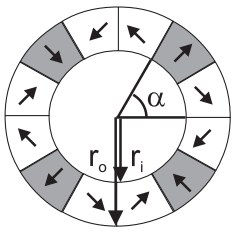

FIG. 1. Design of a miniature PMQ is shown with 12 wedges of permanent magnet. The inner radius of the aperture is r_i = 3 mm and the outer radius is r_o = 10 mm. The arrows point in the magnetization direction.

*Corresponding author.
stefan.becker@physik.uni-muenchen.de

HOMFC. This poses challenges in fabrication of the miniature coil and, in particular, suppressing vibrations during the measurement [12,13]. We present a method allowing the measurement of all relevant magnetic vector field components relying solely on a miniature Hall probe which can be applied to very small apertures at the precision required.

The ability to measure all relevant field components within small apertures allows the introduction of specific HOMFC by changing the position of individual magnet segments. We are thus able to compensate for undesired field components and also deliberately introduce specific components such as octupoles for compensating spherical aberrations or dodecapoles for compensating the effect of fringe fields. In order to minimize the influence of the correction of one field component on the entire field distribution, we apply materials with negligible nonlinear interactions with the magnetic field due to hysteresis effects. Finally, we present measurement results of the tuning of the magnetic field distribution.

II. MEASURING FIELD COMPONENTS

The principle presented here for the measurement of the magnetic field involves a Hall probe.

The magnetic field is scanned in cylindrical coordinates, as shown in Fig. 2: The PMQ is mounted on a rotating stage for controlling the φ coordinate. From the center of rotation, a displacement of the Hall probe along the y axis scans the radial field component B_ρ, whereas the displacement along the x axis scans the azimuthal component B_φ. The offset of $\varphi = 90°$ between B_ρ and B_φ has to be considered.

This method requires the knowledge of the position of the geometrical center of rotation which does not necessarily coincide with the center, i.e., the minimum value, of the magnetic field distribution. The procedure for finding the geometrical center involves a simple feedback algorithm which only requires the Hall probe signal. The result of this iteration is unique as the field changes monotonously from a point inside the aperture.

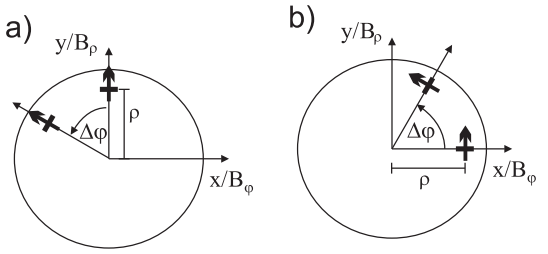

FIG. 2. Scheme of measuring the magnetic vector field in cylindrical coordinates using a Hall probe with the arrow being the surface normal. The radial component (a) as well as the azimuthal component (b) are obtained separately.

A. Fourier analysis

A direct measurement of the entire magnetic field for $0 < \rho < \rho_0$ in cylindrical coordinates inside the aperture overdetermines the magnetic vector field. The assumption of $B_z = 0$ leads to the expansion of the magnetic field using polar coordinates of

$$\vec{B}(\rho, \varphi) = \sum_{l=1}^{\infty} [B_{l\rho}(\rho, \varphi)\vec{e}_\rho + B_{l\varphi}(\rho, \varphi)\vec{e}_\varphi] \qquad (1)$$

with

$$B_{l\rho}(\rho, \varphi) = \rho^{l-1}[a_l \sin(l\varphi) + b_l \cos(l\varphi)] \qquad (2)$$

$$B_{l\varphi}(\rho, \varphi) = \rho^{l-1}[a_l \cos(l\varphi) - b_l \sin(l\varphi)], \qquad (3)$$

a_l and b_l being coefficients representing the HOMFC. The case $B_z \neq 0$ would imply fringe fields, which are discussed in the next section.

Measuring either the B_ρ or the B_φ field component on a single ring [Figs. 3(a) and 3(b)] is sufficient for a complete determination of the magnetic vector field. A Fourier expansion of a ring with the radius ρ_0 leads to the desired coefficients a_l and b_l in magnitude $\sqrt{a_l^2 + b_l^2}$ [Fig. 3(c)] and phase $\arctan(b_l/a_l)$ [Fig. 3(d)] allowing one to construct the vector field [Eq. (1)] using either

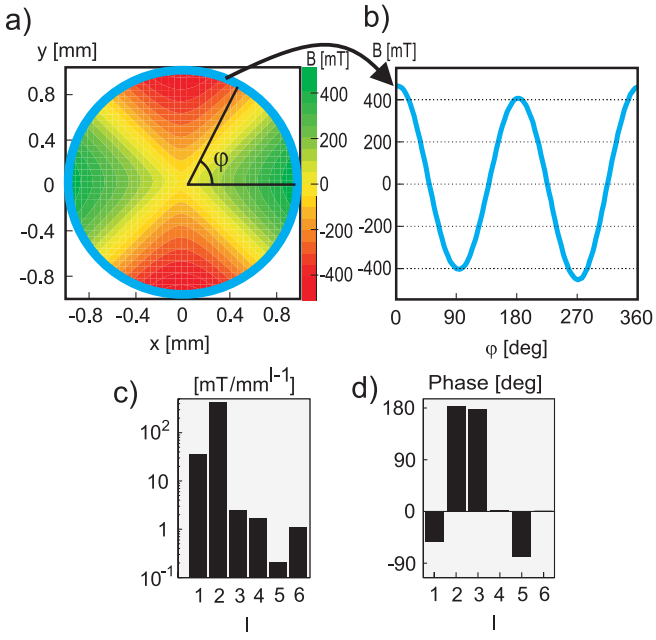

FIG. 3. (Color) Part (a) shows a field measurement using the azimuthal component in cylindrical coordinates and part (b) its outermost ring at $\rho_0 = 1$ mm is plotted against one rotation and used to expand the field coefficients a_l and b_l, shown in (c) magnitude $\sqrt{a_l^2 + b_l^2}$ and (d) phase $\arctan(b_l/a_l)$.

$$a_l = \frac{1}{\pi}\int_0^{2\pi} \rho_0^{1-l} B_\varphi(\rho_0, \varphi)\cos(l\varphi)d\varphi$$
$$b_l = -\frac{1}{\pi}\int_0^{2\pi} \rho_0^{1-l} B_\varphi(\rho_0, \varphi)\sin(l\varphi)d\varphi \quad (4)$$

or

$$a_l = \frac{1}{\pi}\int_0^{2\pi} \rho_0^{1-l} B_\rho(\rho_0, \varphi)\sin(l\varphi)d\varphi$$
$$b_l = \frac{1}{\pi}\int_0^{2\pi} \rho_0^{1-l} B_\rho(\rho_0, \varphi)\cos(l\varphi)d\varphi. \quad (5)$$

B. Proof of principle

The Hall probe used here has a relatively large active probe diameter of 740 μm compared to the aperture of 6 mm. The center of rotation can be determined with micrometer precision in spite of the large probe area. The radius ρ_0 was chosen to be 1 mm, which was the maximum value for the measurements presented here due to the physical size of the entire specific Hall probe device applied. The tilt error of the probe limits the accuracy to sub-5 μm precision for the setup used here. Knowing the absolute positioning error of the geometrical center, we obtain a relative error of $\Delta\rho_0/\rho_0 = 0.5\%$ for $\rho_0 = 1$ mm.

The measurement errors for B_φ or B_ρ and the resolution can be estimated by calculating the remainder:

$$O_k = \int_0^{2\pi} \left| B_{\rho/\varphi}(\rho_0, \varphi) - \sum_{l=1}^{k} B_{l\rho/\varphi}(\rho_0, \varphi) \right| d\varphi. \quad (6)$$

For all field measurements performed, we find contributions of orders up to the sixth (the dodecapole) as is shown by the remainder in Fig. 4(b). This result is expected from the symmetry considerations of the design of the PMQ, but one has to take into account resolution constraints due to the size of the Hall probe, which can make the measurement insensitive to higher order components. Measurement noise or signal drifts would significantly increase the remainder. Such an increase has not been observed in the measurement, indicating that these influences are clearly negligible up to at least the dodecapole order. The maximum order identified by a Hall probe of diameter d_H can be estimated by assuming that the magnetic field is integrated homogeneously over the active area of the probe. An azimuthal variation in field strength as depicted in Fig. 3 can only be resolved if the diameter of the hall probe is smaller than the circumference of the ring of radius ρ_0 over which the variation is measured. For the case considered here with $\rho_0 = 1$ mm and diameter $d_H = 740$ μm, we find that the maximum order component that can be resolved is thus given by $l'_{max} = 2\pi\rho_0/d_H = 8$. Please note that a measurement of the azimuthal field component B_φ does not underlie this resolution limit. For the Halbach quadrupole design only tuning up to the dodecapole ($l = 6$) is required as explained later in Sec. IV. Thus, with the Hall probe available all relevant orders can be resolved, however, one has to consider the measurement error induced by the finite Hall probe size as explained in the following. For each HOMFC l separately one integrates over the active Hall probe surface Ω. The surface has the area $\pi d_H^2/4$ with radial (ρ) or azimuthal (φ) orientation. Using either the coefficient a or b yields the same result. Here, we picked a and obtain

$$B_{\mathrm{int},l,\rho/\varphi}(a_l, \rho, \varphi) = \frac{4}{\pi d_H^2}\int_{\Omega_{\rho/\varphi}} B_{l,\rho/\varphi}(a_l, \rho', \varphi')\cdot dA', \quad (7)$$

with

$$B_{l,\rho}(a_l, \rho, \varphi) = \rho^{l-1} a_l \sin(l\varphi)$$
$$B_{l,\varphi}(a_l, \rho, \varphi) = \rho^{l-1} a_l \cos(l\varphi), \quad (8)$$

following Eq. (3). Using Eqs. (4) and (5) we determine the correction factors,

$$f_{l,\varphi} = \frac{\frac{1}{\pi}\int_0^{2\pi} \rho_0^{1-l} B_{\mathrm{int},l,\varphi}(a_l, \rho_0, \varphi)\cos(l\varphi)d\varphi}{a_l}$$
$$f_{l,\rho} = \frac{\frac{1}{\pi}\int_0^{2\pi} \rho_0^{1-l} B_{\mathrm{int},l,\rho}(a_l, \rho_0, \varphi)\sin(l\varphi)d\varphi}{a_l}. \quad (9)$$

For our case, the factors are given in Table I.

When measuring the radial change in field strength by varying ρ, the Hall probe area integrates over a certain azimuthal variation in φ. This integration yields a value less than the maximum field strength at distance ρ and thus measuring B_ρ underestimates the absolute strength of the HOMFC. For the azimuthal variation the Hall probe inte-

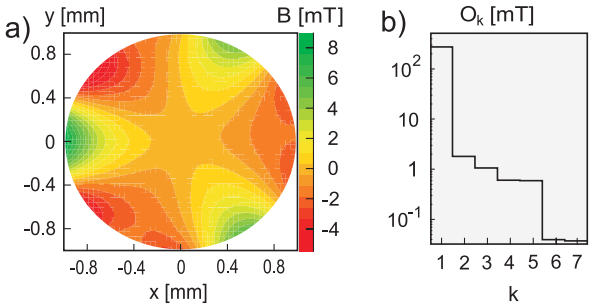

FIG. 4. (Color) Part (a) shows the azimuthal HOMFC from Fig. 3 ($\vec{B} = \sum_{l=3}^{6}[B_{l\rho}(\rho, \varphi)\vec{e}_\rho + B_{l\varphi}(\rho, \varphi)\vec{e}_\varphi]$, note the absolute scale compared to Fig. 3). Part (b) shows the remainder after the kth field component.

TABLE I. Factors f correcting the expanded values of the radial measurement ρ and the azimuthal measurement φ specific to the Hall probe used here.

l	2	3	4	5	6
$f_{l,\rho}$	0.83	0.70	0.54	0.36	0.17
$f_{l,\varphi}$	1	1.05	1.14	1.29	1.49

grates over $B_\varphi(\rho) \propto \rho^{l-1}$ which leads to an overestimation of the HOMFC strength for $l > 2$, since the increase in field strength with increasing distance $\rho > \rho_0$ is not compensated by the reduced field strength measured for $\rho < \rho_0$.

The Hall probe applied here has an enhanced sensitivity in the center of the semiconductor knowing the active Hall probe area. If only the area of the semiconductor is known, one might have to account for an inhomogeneous sensitivity within the area due to the joins to the semiconductor. This is described in [14,15] in detail.

C. Fringe fields

The calculation of the field components from the ring measurement (Fig. 3) requires the assumption of $B_z = 0$ as mentioned before. Hence, the measurement of the ring used for the field expansion must not be performed in the fringes of the field distribution for the expansion following Eq. (1).

There are cases, however, where fringe fields cannot be neglected, in particular when particle beams are being focused to waist sizes on the nanometer scale. Fringe fields are discussed in [3] for Halbach-type PMQs. However, in practice, this does not determine the effect of fringe fields on a beam in a general way. Even if the design of the device and thus the field distribution including the fringe field is known in detail, the final effect on the beam still depends on the length of the PMQ and only works for specific beam properties, which in turn allows the determination of specific HOMFC for compensating the effect of the fringe fields. The method presented here can be used to introduce field components in order to compensate the fringe field.

III. FOCUS MEASUREMENT AT MAMI ELECTRON BEAM

The PMQs as introduced in [1] have been applied at the accelerator MAMI to acquire the imaging quality. These measurements have been carried out prior to the ability to tune the devices. A PMQ lens doublet was used to focus the electron beam. The method of expanding the magnetic field distribution from a Hall probe measurement was applied to reproduce the experimental results.

The beam profile was monitored by a pair of 4 μm wires movable longitudinally in the direction of the beam propagation and transversely through the beam, both in the horizontal and the vertical direction. Bremsstrahlung caused by the beam hitting the wire was detected using an ionization chamber in the forward direction. The Bremsstrahlung's intensity, measured while changing the position of the wires transversely to the beam, determines the beam shape at a certain longitudinal position. The MAMI electron beam can reach energies of up to 855 MeV. We used energies of 270 MeV with an energy stability of $\Delta E/E = 10^{-5}$ and an emittance of 2 nm rad horizontally and 0.7 nm rad vertically.

The calculation of the beam transport involves an expansion of the magnetic fields of the quadrupoles following Eqs. (4) and (5) and tracking the electron beam [16] using the field map given by Eq. (1) and correcting for the Hall probe size following Table I.

The results are shown in Fig. 5 choosing two beam configurations: A convergent electron beam of small size at the entrance of the lens doublet (panel I of Fig. 5), and a

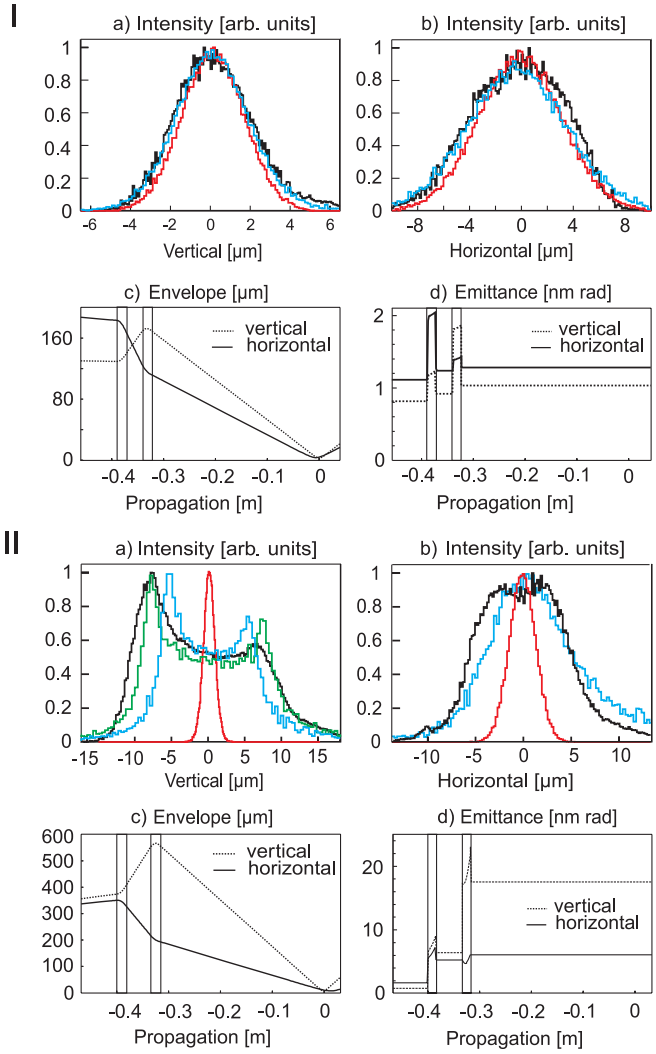

FIG. 5. (Color) Measurements at the Mainz Microtron MAMI are shown with two different beam configurations: The small electron beam configuration (panel I) is shown with the horizontal (Ia) and vertical (Ib) beam plane at the waist. The measured beam (black), the calculated beam using expanded fields (blue), and calculated beam for an ideal quadrupole field (red) are shown for comparison. The calculated beam envelope (Ic) and the emittance (Id) are plotted against the propagation direction of the beam. The vertical lines mark the PMQ positions. The large beam configuration is shown correspondingly (panel II). The green curve in panel IIa is computed from the expanded fields, but with a different focal spot slightly moved towards the PMQs by 1 mm or 0.5% of the focal length.

divergent beam of larger size (panel II of Fig. 5). As expected, the small-beam configuration yields a measured waist size only being a little larger than that of an ideal quadrupole with the same gradient. The waist size of the transport calculation using the expanded fields agrees well with the measured beam waist. The emittance remains virtually constant.

Higher order field components significantly distort the electron beam profile for the large beam configuration, the beam size increases compared to the case of an ideal PMQ doublet, and the form becomes asymmetric as depicted in Ia and Ib of Fig. 5. This distortion is qualitatively described when taking into account the HOMFCs for the computation of the beam evolution. The effect of the HOMFC can also be seen in the evolution of the trace space emittance [17], as is shown in panels Id and IId of Fig. 5. Here, the emittance is deduced from the calculation using the expanded field distribution of the PMQs.

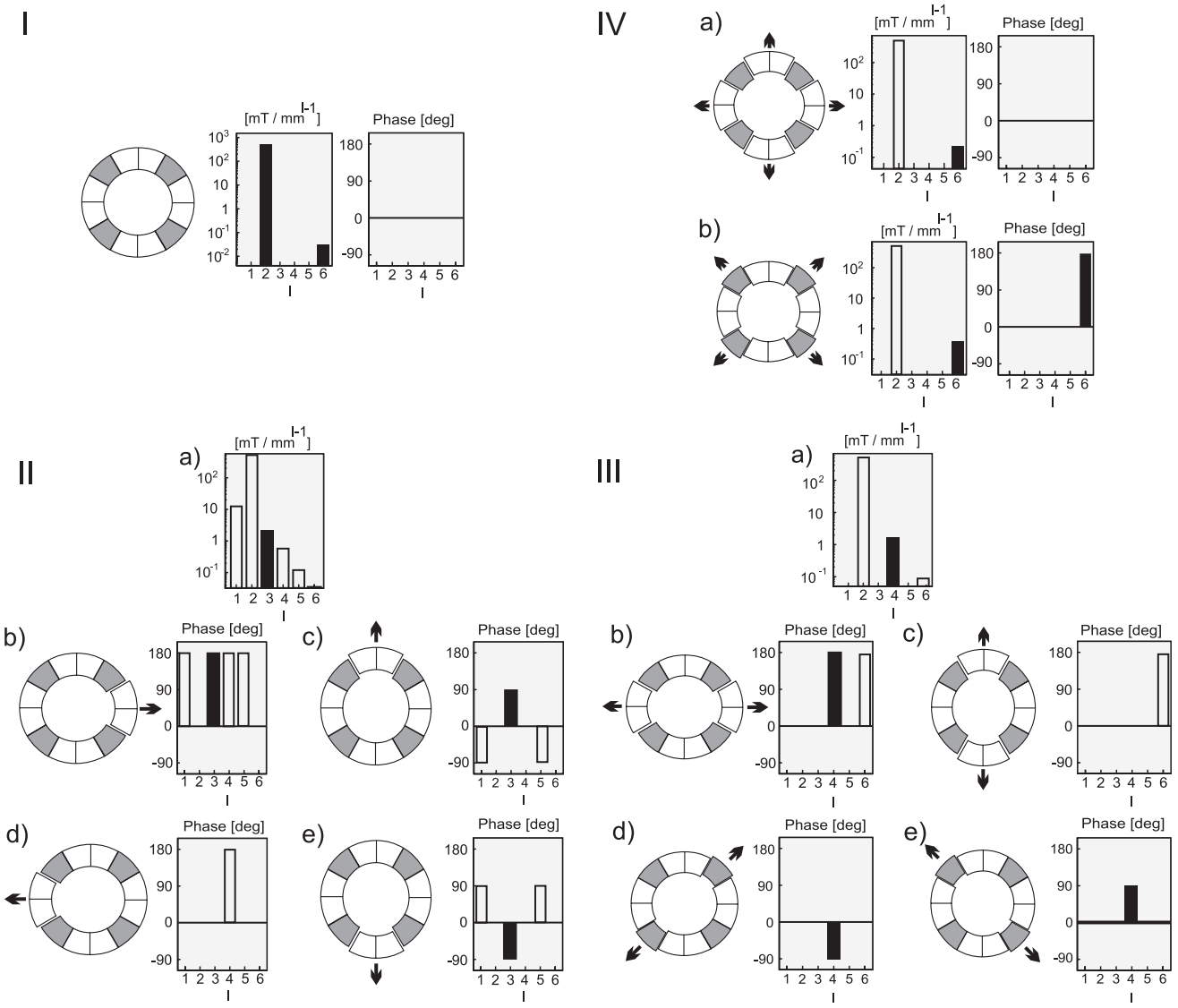

FIG. 6. The introduction of HOMFC with the PMQ having the same orientation as in Fig. 1. Panel I: Magnitude and phases of the calculated magnetic field using the ideal arrangement of permanent magnet wedges. Panel II: Displacing a single pair of tuning wedges by 150 μm introduces a dominant sextupole (IIa). Independent from the specific pairs of tuning wedges displaced, panels IIb–IIe show the effect on the phases of the introduced field components by moving tuning wedges at $\alpha = 0°, 90°, 180°, 270°$. Panel III: Two opposite pairs of tuning wedges are displaced by 150 μm, this introduces a dominant octupole. Panel IIIa shows the effect on the magnitude of the field components. Panel IIIb–IIIc show the effect on the phases of the introduced field components moving tuning wedges at $\alpha = 0°$ and $90°$ affecting a_4. Moving the positioning wedges as shown in panels IIId–IIIe affect b_4. Panel IV: All pairs of tuning wedges are displaced by 150 μm; this introduces a dominant dodecapole. The effect on the magnitudes are shown in panel IVa. Panels IVb and IVc show distinct pairs of tuning wedges which are moved and the effect on magnitudes and phases of the field components. The application of distance holders might be required as in Fig. 7(b).

There can be several reasons for this mismatch, but we constrain ourself to discussing only those effects that have to be considered when aligning the PMQs, namely an offset of the azimuthal angle φ of the lenses with respect to the beam axis and the absolute position of the lens doublet in the lattice. An offset in φ rotating the PMQs by a few hundred μrad already compensates for the absolute difference between measured and calculated beam waist. However, it also significantly distorts the form of the beam profile and can thus be ruled out for the case discussed here. A change in the absolute position of the lens doublet on the subpercent level changes the absolute beam size while maintaining the form of the transverse beam profile, as shown in IIa of Fig. 5, where the lenses are moved 1 mm away from the beam profile monitor, yielding the green curve which matches well the measured profile. This shows that precise measurement and control of the magnetic field as well as precise alignment of the PMQs are required in order to reproduce the computed beam properties in the experiment.

IV. MAGNETIC FIELD TUNING

HOMFC can have a variety of origins, for example, variations of the shape of the wedges or the magnetization direction or strength. The knowledge of the specific origin of an undesired higher order field component is not necessary for its compensation: The introduction of a field component in the same order and magnitude but with a phase shift of 180° leads to its elimination.

Displacing certain wedges introduces well-defined higher order field components which can be used for correcting manufacturing deviations of the wedges, the housing, or for modeling the magnetic field distribution correcting imaging aberrations.

A. Wedge positioning

Figure 7 schematically shows the assembly of permanent magnet wedges within the housing. The four wedges with the magnetic field oriented towards the device axis, which in the following are called positioning wedges, experience centripetal magnetic forces. A thin nonmagnetic cylinder is placed inside the aperture. Its radius determines the radial distance of the wedges from the axis of the device [panels 7(a) and 7(b)]. The positioning wedges are tightened with positioning screws from the housing for fixing the cylinder. The center of the magnetic field can be adjusted to coincide with the geometrical center of the PMQ for the elimination of the dipole field components.

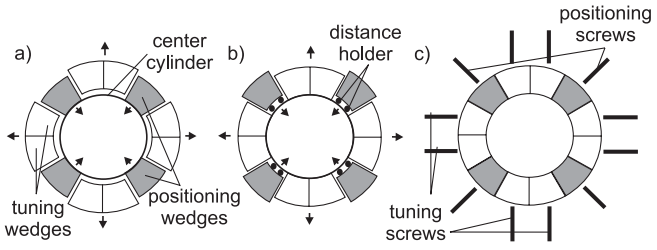

FIG. 7. Part (a) shows an arrangement of permanent magnet wedges and the center cylinder is shown schematically. The arrows point in the direction of the magnetic forces which act centrifugally and centripetally on the wedges. (b) Example for distance holders (e.g. 50–100 μm aluminum foil) of the positioning wedges from the cylinder center. (c) Positioning and tuning screws acting on the wedges.

Magnetic forces centrifugally repel the four remaining pairs of wedges, called tuning wedges in the following. In combination with tuning screws, these forces allow their precise positioning. Since the magnetic forces are acting on the tuning wedges as a pair, the tuning screws are arranged in parallel [panel 7(c)].

B. Introduction of field components

The field distribution is altered by modifying the PMQ by selecting tuning wedges and moving these. The field distribution of a modified PMQ is calculated numerically [18] for obtaining the quantitative effect on individual field components including their phase. The result of the calculation is expanded [Eqs. (4) and (5)] and used for obtaining a table of reference for the effect of moving tuning pairs on the field distribution as shown in Fig. 6.

We first consider the undisturbed quadrupole design in panel I of Fig. 6. Owing to the symmetry of the design, only a dodecapole superimposes on the quadrupole field. Panel II of Fig. 6 shows a dominant sextupole ($l = 3$) which is introduced when moving one pair of tuning wedges. For symmetry reasons, a pure sextupole component cannot be introduced, but an octupole component is also obtained which in turn can be eliminated. The introduction of an octupole component is achieved by moving opposite pairs of wedges as shown in panel III of Fig. 6. Changing b_4 [Eq. (3)] without influencing a_4 requires the movement of the positioning wedges which can be achieved by, e.g., introducing distance holders as is shown in Fig. 7. Alternatively, b_4 can be modified by moving two individual tuning wedges which are arranged at opposite locations from the device center which requires a subsequent compensation of the additionally introduced a_4 component. The introduction of a dodecapole field is shown in panel IV of Fig. 6. Depending on the desired phase, the application of distance holders might be required as is shown in panel 7(b).

C. Adjustment results

Figure 8(a) shows an example of a newly assembled quadrupole. Because of manufacturing deviations of either the wedges or the housing, there is a considerable initial sextupole field component. After compensating for the higher order field components, a much purer quadrupole field is obtained as is shown in Fig. 8, demonstrating the

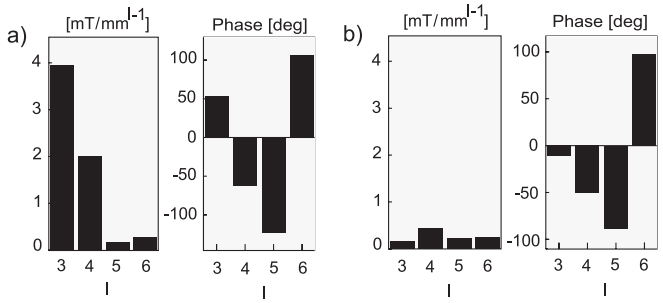

FIG. 8. HOMFC for the proof of principle are illustrated, which are obtained from azimuthal field measurements. Part (a) shows the HOMFC within a newly assembled quadrupole and (b) shows the PMQ tuned with significantly reduced HOMFC. The statistical errors obtained from independent measurements are between 0.1% and 0.7% for the values of the HOMFC, the phases are off between 0.3° and 1°, and are thus negligible.

feasibility of the method discussed. The errors of these measurements correspond to those errors discussed in panel 4(b), since the apparatus used is the same.

V. CONCLUSION

The method presented allows one to shape the magnetic field distribution of a PMQ. The magnetic field distribution is determined from a Fourier expansion of a Hall probe measurement and used as the basis for identifying the tuning wedges to be moved for obtaining the desired field distribution. The precise quantification of HOMFC in conjunction with the complete control of the field configuration allows one to accurately configure the magnetic field distribution to a high degree. After only a few iterations, magnitude and phase of the undesired field components can be reduced significantly. Hence, the control over these field components up to at least the dodecapole allows a larger ratio of the quadrupole's aperture to be illuminated. Moreover, HOMFC such as an octupole or dodecapole can be introduced in order to compensate for imaging aberrations and fringe fields effects.

The advantage of the pure permanent magnet devices over hybrid quadrupole designs lies in the linear superposition of the magnetic field contributions of the individual segments. This allows a decoupled tuning process, and thus a fast and simple adjustment of the magnetic field distribution. The compensation scheme shown here still has potential for improvement since the results presented in this publication were obtained by manually tuning the PMQs. The method for the reduction of HOMFC can easily be automated using simple algorithms which allow one to move the wedges at higher precision.

ACKNOWLEDGMENTS

This work has been funded by the DFG through transregio TR18 and supported by the DFG cluster-of-excellence Munich Center for Advanced Photonics MAP.

[1] T. Eichner, F. Grüner, S. Becker, M. Fuchs, U. Schramm, R. Weingartner, D. Habs, H. Backe, P. Kunz, and W. Lauth, Phys. Rev. ST Accel. Beams **10**, 082401 (2007).
[2] J. K. Lim, P. Frigola, G. Travish, J. B. Rosenzweig, S. G. Anderson, W. J. Brown, J. S. Jacob, C. L. Robbins, and A. M. Tremaine, Phys. Rev. ST Accel. Beams **8**, 072401 (2005).
[3] K. Halbach, Nucl. Instrum. Methods **187**, 109 (1981).
[4] T. Mihara, Y. Iwashita, M. Kumada, and C. M. Spencer, in Proceedings of the 12th Linear Accelerator Conference, Lübeck, Germany, 2004 (SLAC Report No. SLAC-PUB-10878).
[5] C. M. S. Sears, R. L. Byer, E. R. Colby, B. M. Cowan, R. Ischebeck, M. R. Lincoln, T. Plettner, R. H. Siemann, and J. E. Spencer, in Proceedings of the 12th Advanced Accelerator Concepts Workshop, Lake Geneva, Wisconsin, 2005 (SLAC Report No. SLAC-PUB-12422).
[6] M. Schollmeier, S. Becker, M. Geißel, K. A. Flippo, A. Blažević, S. A. Gaillard, D. C. Gautier, F. Grüner, K. Harres, M. Kimmel, F. Nürnberg, P. Rambo, U. Schramm, J. Schreiber, J. Schütrumpf, J. Schwarz, N. A. Tahir, B. Atherton, D. Habs, B. M. Hegelich, and M. Roth, Phys. Rev. Lett. **101**, 055004 (2008).
[7] S. P. D. Mangles, C. Murphy, Z. Najmudin, A. Thomas, J. Collier, A. Dangor, E. Divall, P. Foster, J. Gallacher, C. Hooker, D. Jaroszynski, A. Langley, W. Mori, P. Norreys, F. Tsung, R. Viskup, B. Walton, and K. Krushelnick, Nature (London) **431**, 535 (2004).
[8] C. G. R. Geddes, C. Toth, J. van Tilborg, E. Esarey, C. Schroeder, D. Bruhwiller, C. Nieter, J. Cary, and W. Leemans, Nature (London) **431**, 538 (2004).
[9] J. Faure, Y. Glinec, A. Pukhov, S. Kiselev, S. Gordienko, E. Lefebvre, J.-P. Rousseau, F. Burgy, and V. Malka, Nature (London) **431**, 541 (2004).
[10] F. Grüner, S. Becker, U. Schramm, T. Eichner, M. Fuchs, R. Weingartner, D. Habs, J. Meyer-ter-Vehn, M. Geissler, M. Ferrario, L. Serafini, B. an der Geer, H. Backe, W. Lauth, and S. Reiche, Appl. Phys. B **86**, 431 (2007).
[11] Vacuumschmelze Hanau, Vacodym 764 HR data sheets (2005), www.vacuumschmelze.com.
[12] G. Datzmann, G. Dollinger, G. Hinderer, and H.-J. Körner, Nucl. Instrum. Methods Phys. Res., Sect. B **158**, 74 (1999).
[13] Y. Iwashita, T. Mihara, M. Kumada, and C. M. Spencer, *Proceedings of the 21st Particle Accelerator Conference, Knoxville, 2005* (IEEE, Piscataway, NJ, 2005).
[14] I. Hlásnik and J. Kokavec, *Hall Generator in Inhomogenous Field and Dipole Notion of the Hall Effect*, Solid State Electronics (Pergamon Press, New York, 1966), Vol. 9, pp. 585–594.
[15] V. Yu. Korovkin, Izmeritel'naya Tekhnika **8**, 50 (1988).
[16] General Particle Tracer, www.pulsar.nl.
[17] K. Flöttmann, Phys. Rev. ST Accel. Beams **6**, 034202 (2003).
[18] CST EM Studio, www.cst.com.